

Light Propagation in Transparent Wood: Efficient Ray-Tracing Simulation and Retrieving an Effective Refractive Index of Wood Scaffold

Jiu Pang, Adil Baitenov, Céline Montanari, Archana Samanta, Lars Berglund, Sergei Popov,* and Igor Zozoulenko*

Transparent wood (TW), a biocomposite material demonstrating optical transparency in the visible range, has attracted much interest in recent years due to great potential for ecofriendly applications, for instance, in construction industry and functionalized organic materials. Optical properties of TW, including transparency and haze, depend on a particular structure of cellulose-based backbone compound, (mis-)matching of the refractive indices (RIs) between TW compounds, and the polymer matrix. Although there are data of cellulose RIs for various forms of cellulose (fibers, powder, hot-pressed films, etc.), these values might differ from an effective RI of the TW substrate. Herein, a numerical model of light propagation in the TW, based on the real cellular structure in wood, is presented and applied to estimate an effective RI of the delignified wood reinforcement in the experimentally investigated TW material. Ray-tracing and rigorous electromagnetic approaches are compared for modeling light propagation in the TW. Ray tracing demonstrates considerably simplified yet accurate and efficient solutions. The work brings substantial progress toward realistic and practical wood modeling for the purpose of applications, materials design, and fundamental studies.

wood) in Figure 1a.^[1] This structure is a basis for mechanical strength needed in numerous applications, first of all, load-bearing construction materials.^[2,3] The complex porosity and anisotropic structure of TW result in complex light scattering and, as a consequence, strong nonhomogenous haze, which can be both favorable or disadvantageous depending on particular applications.^[4–7]


Hardwood generally includes 20–25% lignin, 40–45% cellulose, and 25–30% hemicellulose.^[1] TW is fabricated in several steps, starting with the delignification of a wood template, followed by removal of lignin, which, in turn, is the main component absorbing light in a wood structure.^[8,9] The obtained delignified wood substrate is primarily composed of holocellulose (cellulose and hemicelluloses). Next, a polymer material (PMMA, thiol-ene, or similar) with a refractive index (RI) closely matching the wood template is infiltrated in the delignified wood.^[4,9,10] The polymer

impregnation is implemented to decrease the light scattering inside the material, which originates on interfaces between holocellulose (main component of the delignified wood) structure and air voids always existing inside TW.^[4] One of the challenges is the mismatch of RIs of filling polymers and wood reinforcement in TW materials, which causes light scattering.^[9] The optional process called acetylation can be conducted to improve the surface compatibility between filling polymer and

1. Introduction

Transparent wood (TW) is a novel material that is based on natural wood, keeping its mechanical properties and bringing new functionality—high optical transparency.^[1–6] It keeps the hierarchical structure of natural wood, which consists of cellulose fibers (nanofibrils and assembling fibers, 10–70 μm diameter), vessels (200–700 μm diameter), and rays, as shown (for balsa

J. Pang, I. Zozoulenko
Wallenberg Wood Science Center
Laboratory of Organic Electronics
Department of Science and Technology
Linköping University
Norrköping SE-60174, Sweden
E-mail: igor.zozoulenko@liu.se

 The ORCID identification number(s) for the author(s) of this article can be found under <https://doi.org/10.1002/adpr.202100135>.

© 2021 The Authors. Advanced Photonics Research published by Wiley-VCH GmbH. This is an open access article under the terms of the Creative Commons Attribution License, which permits use, distribution and reproduction in any medium, provided the original work is properly cited.

DOI: 10.1002/adpr.202100135

A. Baitenov, A. Samanta, S. Popov
Department of Applied Physics
School of Engineering Science
KTH Royal Institute of Technology
SE-11419 Stockholm, Sweden
E-mail: sergeip@kth.se

C. Montanari, L. Berglund
Wallenberg Wood Science Center
Department of Fiber and Polymer Technology
KTH Royal Institute of Technology
Teknikringen 56, SE-10044 Stockholm, Sweden

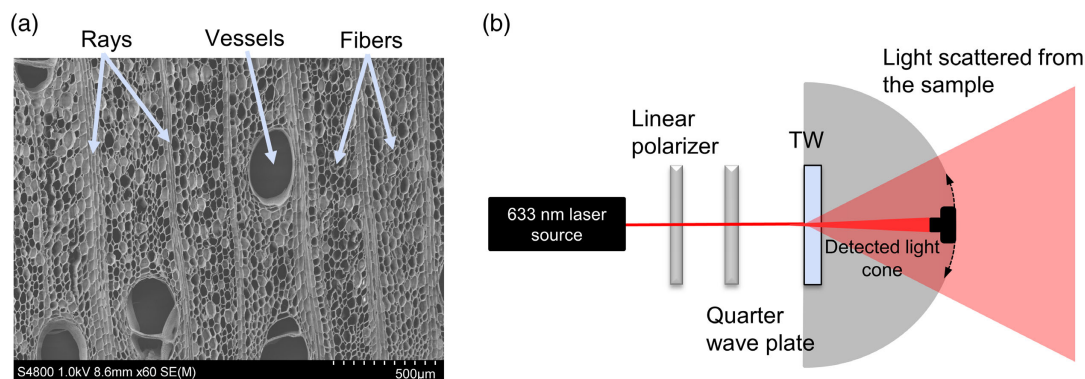


Figure 1. a) Cross-sectional SEM image of balsa wood highlighting the wood structural components (fibers, vessels, and rays). b) Schematic diagram of experimental setup.

holocellulose, which decreases light scattering.^[11] An alternative solution is implementing bleaching process with suitable polymers, for example, thiol-ene, rather delignification, where the lignin is retained in the wood but does not absorb light anymore. This approach can improve polymer adhesion and decrease voids between polymer and wood scaffold. Another challenge is production of samples thicker than 1 cm, due to surface damage of TW during delignification process, which depends on the thickness of the sample.^[4,12]

Currently, research on TW is mostly focused on developing production techniques, such as improvement of mechanical properties, increase in the maximum size of samples, and functionalization via embedding of various compounds.^[13–16] Functionalized TW has potential applications in smart buildings, functionalized biodegradable materials for decoration, design, photovoltaics, thermal shielding, and others.^[4,17,18] Improving optical properties, minimizing haze, or combining high transmittance and high haze^[7] are also interesting for TW development. However, the RI of holocellulose has an average, or “effective,” value due to the complex inherent structure and birefringence of the material.^[9] To get detailed insight into light propagation and scattering in the TW, a method to reliably estimate the effective RI of the wood substrate is required to select a polymer with an appropriate RI matching the host template. There are various experimental methods for RI measurement of holocellulose in the condensed/dense form (fibers, powder, pressed, etc.).^[19–23] However, such values might differ from an effective RI of the TW, which is of practical importance for the application development. The RI of delignified wood can also be estimated using solvent-assisted methods,^[24] although considerable experimental work is required.^[14–17] However, the RI obtained from such measurements depends on a particular wood species.

In contrast, to retrieve the value of an effective RI, the detailed simulation of light propagation in wood template (with or without various structure modifications), a full-scale model taking into account many physical properties, is required. Although various simulation approaches were previously implemented, they mainly tackle unmodified wood structure and are based on the use of stochastic models^[25–28] rather than rigorous numerical models.

In this work, we present a model that upon comparison with experimental results allows estimation of an effective RI in TW materials. The model implements ray-optics calculations using

the finite-element method in COMSOL Multiphysics, which were validated and compared with rigorous wave-optics calculations (also using COMSOL). The ray-optics analysis demonstrates its capability of modeling complex, cellular TW microstructures with significantly less computational power, making it possible to model large-scale structures. The model can predict light propagation and angular distribution in samples with different wood cell structures, and parameters such as thickness, polymer RI, and wood types can be varied for material design purposes.

2. Simulations

2.1. TW Modeling Approach

The COMSOL Multiphysics 5.5 was used for studying optical properties of TW materials. To generate a model mesh corresponding to a realistic TW, SEM images of a TW sample were studied, as shown in **Figure 2a**. Due to strong light scattering upon its propagating through the sample, the light-wave front creates a light cone. Thus, the width of the modeled area of the sample also gradually increases for the samples with larger thickness (as shown in **Figure 2a**). Thus, it is reasonable to use the trapezoid shape for the modeling area to save the computer resources. In the experimental study, the direction of incident light beam was inclined by about 45° angle to the direction of structural rays inside the TW sample. Thus, we implemented the COMSOL model with a 45° angle between structure rays and incident light to keep the consistency between experiments and simulations. The width of the incident beam was about 400 µm, and the TW models with 1, 2, and 3 mm material thicknesses were considered. An exact shape of the intensity curves (both in simulations and in experiments) depends on the particular position of the incident beam and its propagating path through the sample, that is, fiber–vessel–ray composition. To make the intensity curves smoother and less dependent on these factors, models for each thickness were run three times using different areas from SEM images (**Figure S2–S4**, Supporting Information), and the final results have been averaged for each thickness, respectively. Large-area SEM images for each case were obtained from merging four high-resolution images (shown as white border lines in **Figure 2a**). To model the TW,

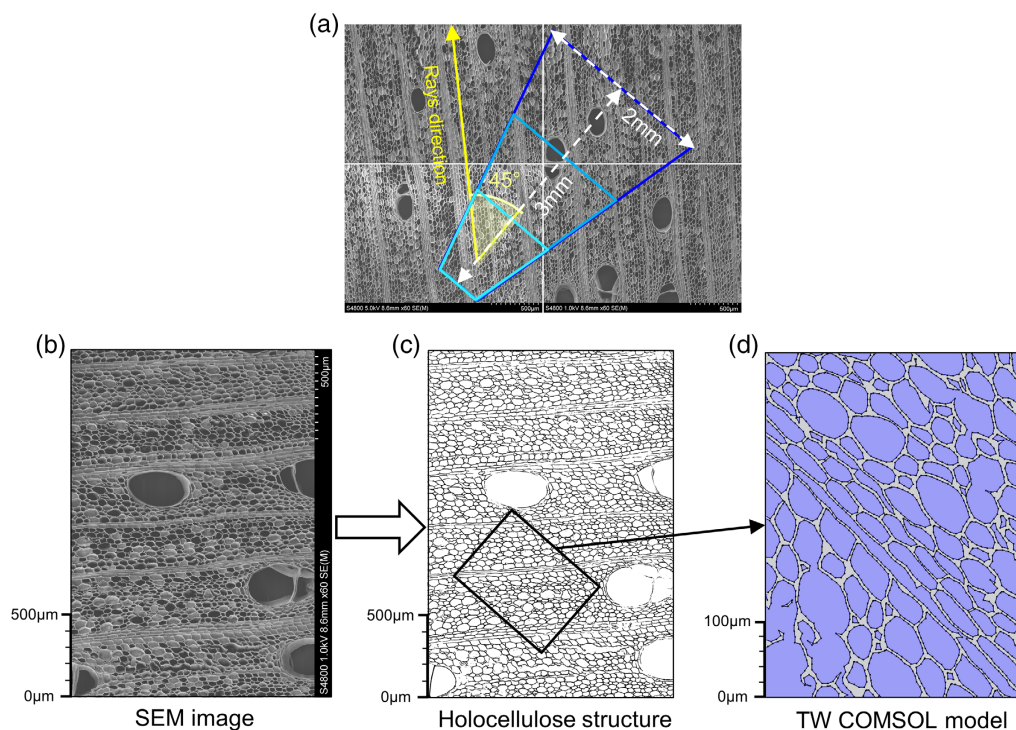


Figure 2. a) Schematic diagram of sizes and directions of TW COMSOL modeling with SEM images. Three samples of different TW thicknesses, 1, 2, and 3 mm, are shown by light blue, blue, and dark blue, respectively. b–d) The modeling process from SEM image to TW models.

we use a 2D model. We estimate that the effect of 3D scattering is within 0.1–1%, and therefore it can be safely neglected, see Section S1 and Figure S1, Supporting Information for details.

To transfer a real SEM image into a model mesh and properly distinguish TW structural details, the Trainable Weka Segmentation plugin in ImageJ was used,^[29] see Figure 2b,c. As shown in Figure 2d, the gray and purple regions represent the wood (holocellulose) reinforcement and filling polymer, thiol-ene, respectively. The interfaces of the TW structures are formed by closed curves. Each closed curve is represented by polygons with a limited number of connecting points, see Figure 2d. As the tremendous amount of data of meshing coordinates requires very large amount of computer memory to generate the models, the vortex distance in each polygon (i.e., the distance between the connecting points in Figure 2d) should be carefully chosen. The TW models using vortex distances of 5, 7, 9, and 12 μm were tested. When the vortex distances of the polygons were changed from 5 to 9 μm , the angular distribution of the normalized intensity and its full width at half maximum (FWHM) are affected very little, as shown in Figure S5, Supporting Information. Thus, in our simulations, we used the 7 μm vortex distance, which represents a good compromise between the accuracy of the results and the memory requirements.

2.2. Comparison of Simulation Methods: Wave Optics versus Ray Optics

To simulate angular distribution of the transmitted light, a rigorous electromagnetic model based on the solution of the

Maxwell equations should be implemented in a general case, because the TW material is of very complex structure with feature sizes ranging from nanometers to tens of micrometers. However, for the samples of a practical size, that is, with thickness of several millimeters, the rigorous approach is not feasible due to fast growth of the number of mesh elements needed to reconstruct the sample geometry. In contrast, it is reasonable to expect that total contribution of small-scale details to light scattering (considerably less than the light wavelength, in the Rayleigh scattering domain) is negligible, and mainly scattering on larger material details (order of wavelength and larger, e.g., Mie scattering) would generate an appropriate light distribution pattern. Thus, if the impact of material details on the subwavelength scale on light propagation can be neglected, the ray-tracing approach can be used to obtain sensible results with much less computational resources. To validate the possibility of using the ray-tracing method, we compared simulation results for small-sized models for both rigorous electromagnetic and ray-tracing modeling. For the wave-optics simulations, we used “Frequency Domain Electromagnetic Waves” interface in the “Wave Optics” modulus in COMSOL, whereas “Ray Tracing” interface in the “Ray Optics” modulus was used for the ray-optics simulations.

To build the modeling space, we consider the half-circle working area with a sample placed in the center of the domain, whereas the transmitted light is determined on the arc line enclosing the working area (Figure 3), which is a good representation of the experimental setup. To minimize data of the geometrical mesh, we implemented a trapezoidal shape for light cone propagation in the material, as explained in the previous section (Figure 2a).

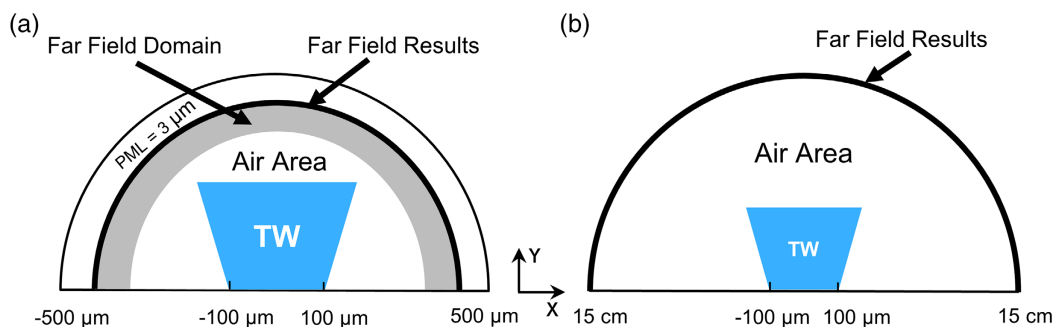


Figure 3. Schematic diagram of models for a) wave- and b) ray-optics calculations. The far field results in the diagram show the position where angular distributions of intensities are counted.

Figure 3a,b shows the diagram models for wave-optics and ray-optics simulation, respectively. For wave-optics simulation, the TW structure was placed in the near-field region to study light propagation, and the far-field calculation was used to obtain the angular distributions of light intensity.^[30,31] For this method, the perfectly matched layer (PML) must be imposed to absorb waves backscattered from the boundary of the working area.^[32] Light waves are defined by an electric field, and the scattered light also consists of plane waves. The mesh size needs to be five times smaller than the light wavelength to guarantee an appropriate wave propagation for wave-optics simulation.

In ray-optics calculations, a larger model, which contains TW structures in the near-field region and propagating distance to 15 cm, was built, maintaining consistency with the experimental setup. For ray-optics calculations, the incident light is realized as a bunch of optical rays incident in the y -direction from a segment ranging from -75 to $75 \mu\text{m}$ in x -coordinate with the $0.01 \mu\text{m}$ step, see **Figure 4a**. The maximum number of reflected rays (total internal reflection is not included) is set to 1 million, and due to the compositional and structural complexities of TW models, the reflected rays are controlled by setting the reflection threshold, that is, the reflected rays are included unless the power of the reflected ray is less than 1% of the initial ray.

As a starting point to validate both models, we used a simplified geometry of the TW structure, where the holocellulose components are represented by ring areas, and the filling polymer (thiol-ene) occupies areas inside and outside the rings, see

Figure 4a,b. The RIs of the holocellulose and thiol-ene are, respectively, 1.54 and 1.56.^[10] The centers of the rings and their diameters ($20\text{--}30 \mu\text{m}$) are chosen randomly. The model geometry is produced by Java code in the Method Editor of COMSOL. Further details and the Java code are attached in Supporting Information. The gray area outside the trapezoid (propagating light cone) represents air, where optical waves pass through and reach the far-field region.^[11] The centers of the rings and their diameters ($20\text{--}30 \mu\text{m}$) are chosen randomly. The model geometry is produced by Java code in the Method Editor of COMSOL. Further details and the Java code are attached in Supporting Information. The gray area outside the trapezoid (propagating light cone) represents air, where optical waves pass through and reach the far-field region.

Finally, the angular distribution of light intensity is calculated in the far zone in 300 measurement points for angular distribution. Upon propagating through the thin TW sample ($400 \mu\text{m}$), the resulting light intensity is not sufficiently averaged by scattering, so, the angular distribution curves show explicit ripples. To avoid such artifacts, ten TW models were generated, and the light propagation was calculated by averaging corresponding intensity distribution. This approach was implemented for both wave- and ray-optics cases. To test the wave-optics calculations, the wavelength of incident light was set to $1 \mu\text{m}$, and the memory requirement in the computation process exceeded 100 GB.

Figure 4c shows the averaged normalized intensity for wave- and ray-optics simulations. Both approaches lead to the

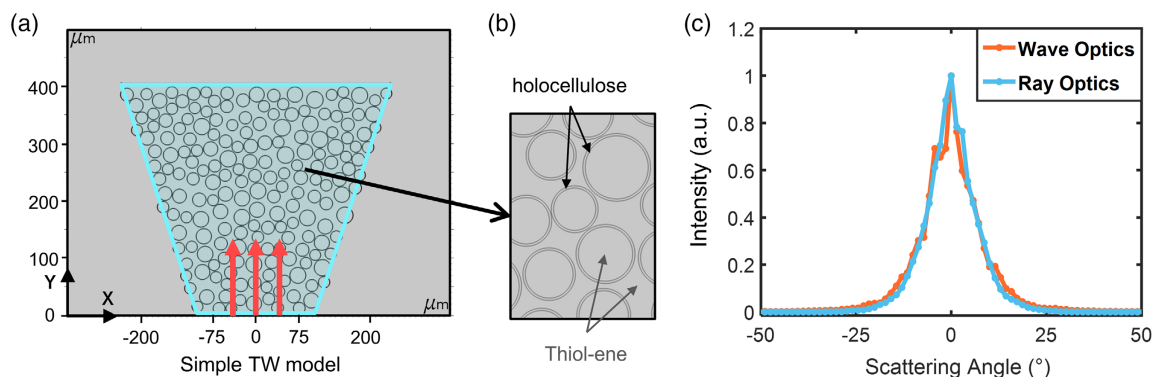


Figure 4. a) Simplified TW model and b) its partial enlarged view. Red arrows indicate the direction of light. c) Averaged normalized intensity curves of wave- and ray-optics calculations.

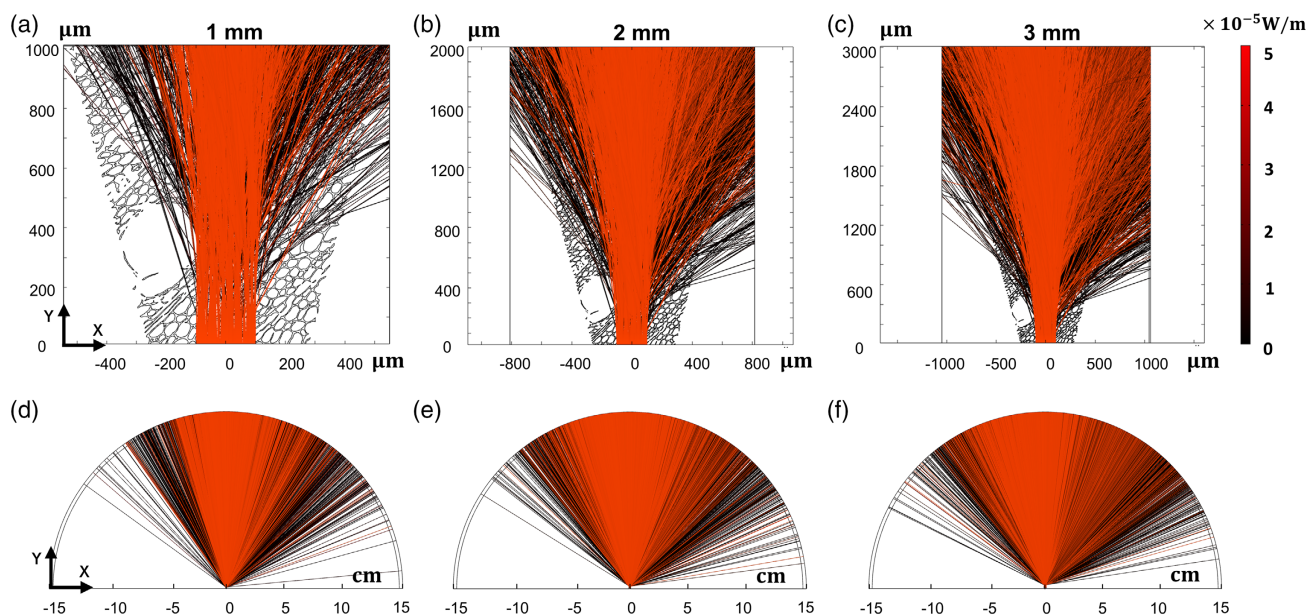


Figure 5. Ray tracing for different TW thicknesses: a,d) 1 mm, b,e) 2 mm, and c,f) 3 mm. Top and bottom figures show near-region and far-region results, respectively. The optical power transported by optical rays ranging from 0 to $5 \times 10^{-5} \text{ W m}^{-1}$ is represented by color bar encoding from black to red. In these simulations, the thiol-ene polymer matrix has $\text{RI} = 1.56$, and the cellulosic wood substrate has $\text{RI} = 1.54$.

angular intensities of the same shape. Note that in the central direction (range of $\approx \pm 20^\circ$), the wave simulation exhibits stronger oscillation. It is noteworthy that not only the shapes of the normalized intensities for wave- and ray-optics calculations are very similar but absolute values of the calculated transmittance are also very close (90.9% and 89.0%, respectively). This is most probably attributed to strong interference effects still noticeable on such a short propagation distance. After all, the good matching between the wave- and ray-optics calculations proves the validity of the latter approach.

3. Results and Discussion

The optical power obtained by the ray-tracing simulations for TW samples of different thicknesses is shown in **Figure 5a–c** in the near zone (i.e., the sample region) and in **Figure 5d–f** in the far zone, for 1, 2, and 3 mm-thick TW samples, respectively. Light is progressively scattered while propagating through the modeled TW sample. As the thickness increases, the scattering area becomes wider, as shown in **Figure 5a–c**. It is worth noticing that a certain percentage of rays reaches the left or right boundaries inside the working area of the model is neglected, affecting the angular intensity distribution in the far field, as will be discussed later.

The angular distributions of normalized intensity, experimental measurements, and ray-optics simulations are shown in **Figure 6**. For simulation results, various values of holocellulose RIs are tested to obtain the best fit to the experimental data, that allows to retrieve an effective RI of the wood compound in the TW material. As shown in **Figure 6a–c**, the normalized intensity curves for all TW samples (1, 2, and 3 mm) exhibit the best agreement with the experiment results when the RI of holocellulose is set to $n = 1.54$. Note that for thicker samples (2 and 3 mm) the

simulation results deviate from the experimental data for larger scattering angles ($> |25^\circ|$). This discrepancy originates from the power loss of scattered light that reaches the left and right sides of the TW model. As shown in **Table 1**, the rays bouncing in the left and right sides contain about 10.62% of light intensity for 3 mm TW models, which is much larger than for the 1 mm (1.10%) and 2 mm (4.40%) TW samples. Thus, we can conclude that the effective RI of holocellulose in TW samples is better approximated with value of 1.54 ± 0.005 . (Note that the RIs $n = 1.53$ and $n = 1.55$ provide the intensity profiles that are quite distinct from the case of the best fit $n = 1.54$; therefore, we estimate the error as $\Delta = (1.55 - 1.54)/2 = (1.54 - 1.53)/2 = 0.005$.) One may note that the model can also be used to estimate scattering effects from polymers of different RIs.

The total transmittance of the TW material decreases gradually with increased TW thickness, due to increased light scattering during light propagation through the material, and the transmittance of 1, 2, and 3 mm samples reaches 93.48%, 89.52%, and 82.55%, respectively. Here, the true transmittance of the 3 mm TW model is underestimated due to the intensity loss on the left and right sides of the fairly narrow TW model. In addition, the reflectivity for 1–3 mm TW is about 4.74%.

4. Conclusion

In this article, we report the modeling method of TW samples to study light propagation and estimate an effective RI for such materials. First, to investigate the importance of the interference and diffraction effects, the wave- and ray-optics calculations for a simplified TW model were carried out using COMSOL Multiphysics. Both methods demonstrated good agreement, which validates the utilization of the ray-tracing technique and

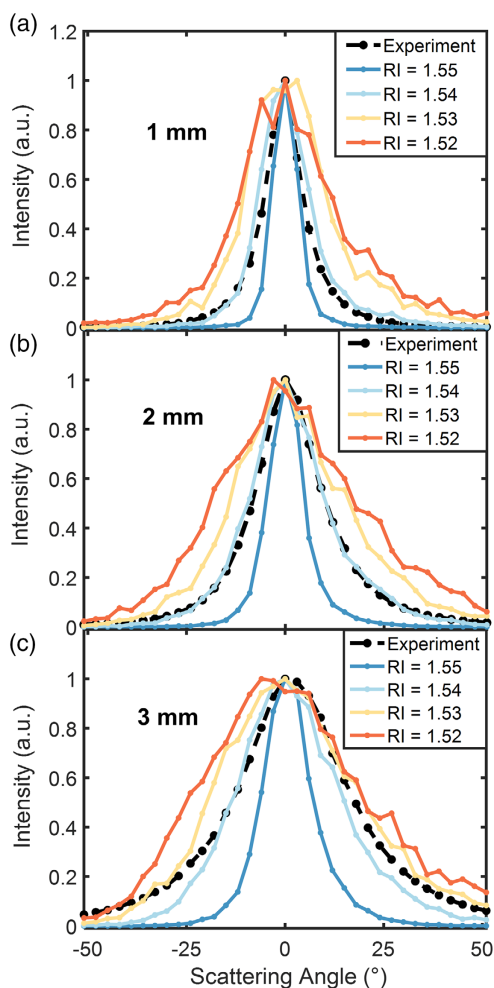


Figure 6. The angular distributions of normalized intensity curves of experimental measurements and ray-optics calculations for a) 1 mm, b) 2 mm, and c) 3 mm TW materials. RI represents the refractive index of holocellulose used in the ray-optics calculations.

Table 1. Relative intensity of optical rays reaching the top, below, left, and right sides of the modeling area, when RI of holocellulose is 1.54. The TW model losses show the amount of optical power lost due to the missing rays that cannot reach the region corresponding to where they contribute to the measured signal. It happens due to the limited width of simulation area. The reflected rays are not included if the reflected intensity is less than 0.1% of the incident ray.

Relative intensity of optical rays [%]	Top wall	Bottom wall	Left wall	Right wall	Reflected loss	TW model loss
1 mm	93.48%	4.74%	0.07%	1.03%	0.68%	1.10%
2 mm	89.52%	4.74%	0.53%	3.87%	1.34%	4.40%
3 mm	82.55%	4.74%	1.64%	8.98%	2.09%	10.62%

its application for the extraction of the RI of the TW materials. Then, a realistic model of TW was designed using SEM images obtained from the TW samples tested in our experiments. Ray-optics simulation of the intensity angular distribution of light propagating through the TW samples is in good agreement

with the experimental measurements. This allows retrieving of the efficient RI of the TW material, which is shown to be 1.54 ± 0.005 for the 633 nm light source. The ray-tracing approach implemented with an finite element method (FEM) model demonstrates excellent accuracy and, at the same time, efficiency and simplicity for modeling such complex structures as TW materials. It can be used for material design purposes and for interpretation of experimental scattering phenomena. The modeling method is also feasible for other transparent cellulosic materials.

5. Experimental Section

The modeling idea was to retrieve TW material (effective) RI as a fitting parameter to match experimental measurements with simulation results.

The experimental setup consisted of 633 nm He–Ne laser, a linear polarizer (LP), quarter-wave plate (QWL), and a power detector with angular displacement to detect scattered light after the TW sample, see Figure 1b. As the light distribution after transmission through the TW sample depended on polarization and alignment of the sample, LP and QWL were installed to provide the circular polarization incident on the sample and minimize the impact of polarization.

The power meter was moved along an arc trajectory with 3° steps to avoid overlap of collected light cones for every measured point. In this experiment, bleached balsa wood samples of thicknesses ranging from 1 to 5 mm were studied. Experimental results were compared with modeling for samples up to 3 mm in thickness, as modeling of thicker samples was limited by computer memory requirements. More details about experiments and fabrication of TW samples are given in previous works.^[10,33] Scanning electron microscopy (SEM) images of the wood morphology were acquired from balsa wood cross sections using a field-emission scanning electron microscope (FESEM, Hitachi S-4800, Japan). The cross sections were obtained by sectioning the samples in the wet state using a microtome (Leica SM2010 R Sliding Microtome, Germany), followed by critical point drying (Autosamdri-815, Tousimis, USA). All samples were sputter coated (Cressington R308, UK) with a thin layer of Pt/Pd prior to imaging.

Supporting Information

Supporting Information is available from the Wiley Online Library or from the author.

Acknowledgements

The computations were conducted on resources provided by the Swedish National Infrastructure for Computing (SNIC) at NSC and HPC2N. The authors acknowledge funding from the European Research Council Advanced Grant, project no. 742733, Wood NanoTech, and Knut and Alice Wallenberg foundation through the Wallenberg Wood Science Center at KTH Royal Institute of Technology and Linköping University.

Conflict of Interest

The authors declare no conflict of interest.

Data Availability Statement

The data supporting the findings of this study are available within the article and its supplementary materials.

Keywords

ray optics simulations, refractive index, transparent wood, wave optics simulations

Received: May 19, 2021

Revised: July 8, 2021

Published online: August 26, 2021

- [1] M. Borrega, P. Ahvenainen, R. Serimaa, L. Gibson, *Wood. Sci. Technol.* **2015**, 49, 403.
- [2] C. Chen, Y. Kuang, S. Zhu, I. Burgert, T. Keplinger, A. Gong, T. Li, L. Berglund, S. J. Eichhorn, L. Hu, *Nat. Rev. Mater.* **2020**, 5, 642.
- [3] M. Zhu, J. Song, T. Li, A. Gong, Y. Wang, J. Dai, Y. Yao, W. Luo, D. Henderson, L. Hu, *Adv. Mater.* **2016**, 28, 5181.
- [4] Y. Li, E. Vasileva, I. Sychugov, S. Popov, L. Berglund, *Adv. Opt. Mater.* **2018**, 6, 1800059.
- [5] Y. Huang, Y. Chen, X. Fan, N. Luo, S. Zhou, S. C. Chen, N. Zhao, C. P. Wong, *Small* **2018**, 14, 1801520.
- [6] E. Vasileva, H. Chen, Y. Li, I. Sychugov, M. Yan, L. Berglund, S. Popov, *Adv. Opt. Mater.* **2018**, 6, 1800999.
- [7] G. Jacucci, L. Schertel, Y. Zhang, H. Yang, S. Vignolini, *Adv. Mater.* **2020**.
- [8] Y. Wu, J. Zhou, Q. Huang, F. Yang, Y. Wang, X. Liang, J. Li, *ACS omega* **2020**, 5, 1782.
- [9] Y. Li, Q. Fu, S. Yu, M. Yan, L. Berglund, *Biomacromolecules* **2016**, 17, 1358.
- [10] M. Höglund, M. Johansson, I. Sychugov, L. A. Berglund, *ACS Appl. Mater. Interfaces* **2020**, 12, 46914.
- [11] Y. Li, X. Yang, Q. Fu, R. Rojas, M. Yan, L. Berglund, *J. Mater. Chem. A* **2018**, 6, 1094.
- [12] H. Chen, A. Baitenov, Y. Li, E. Vasileva, S. Popov, I. Sychugov, M. Yan, L. Berglund, *ACS Appl. Mater. Interfaces* **2019**, 11, 35451.
- [13] X. Wang, T. Zhan, Y. Liu, J. Shi, B. Pan, Y. Zhang, L. Cai, S. Q. Shi, *ChemSusChem* **2018**, 11, 4086.
- [14] L. A. Berglund, I. Burgert, *Adv. Mater.* **2018**, 30, 1704285.
- [15] Y. Li, Q. Fu, R. Rojas, M. Yan, M. Lawoko, L. Berglund, *ChemSusChem* **2017**, 10, 3445.
- [16] Y. Li, X. Yang, Q. Fu, R. Rojas, M. Yan, L. Berglund, *J. Mater. Chem. A* **2018**, 6, 1094.
- [17] Y. Li, M. Cheng, E. Jungstedt, B. Xu, L. Sun, L. Berglund, *ACS Sustain. Chem. Eng.* **2019**, 7, 6061.
- [18] Y. Li, S. Yu, J. G. C. Veinot, J. Linnros, L. Berglund, I. Sychugov, *Adv. Opt. Mater.* **2017**, 5, 1600834.
- [19] I. Niskanen, T. Suopajärvi, H. Liimatainen, T. Fabritius, R. Heikkilä, G. Thungström, *J. Quant. Spectrosc. Radiat. Transf.* **2019**, 235, 1.
- [20] M. Boccara, Y. Fedala, C. V. Bryan, M. Bailly-Bechet, C. Bowler, A. C. Boccara, *Biomed. Opt. Express* **2016**, 7, 3736.
- [21] J. L. H. Chau, Y. M. Lin, A. K. Li, W. F. Su, K. S. Chang, S. L. C. Hsu, T. L. Li, *Mater. Lett.* **2007**, 61, 2908.
- [22] G. Knöner, S. Parkin, T. A. Nieminen, N. R. Heckenberg, H. Rubinsztein-Dunlop, *PRL* **2006**, 97, 157402.
- [23] C. Lü, C. Guan, Y. Liu, Y. Cheng, B. Yang, *Chem. Mater.* **2005**, 17, 2448.
- [24] H. Chen, C. Montanari, M. Yan, S. Popov, Y. Li, I. Sychugov, L. A. Berglund, *RSC Adv.* **2020**, 10, 40719.
- [25] C. D'Andrea, A. Farina, D. Comelli, A. Pifferi, P. Taroni, G. Valentini, R. Cubeddu, L. Zoia, M. Orlandi, A. Kienle, *Appl. Spectrosc.* **2008**, 62, 569.
- [26] A. Kienle, C. D'Andrea, F. Foschum, P. Taroni, A. Pifferi, *Opt. Express* **2008**, 16, 9895.
- [27] M. Ban, T. Inagaki, T. Ma, S. Tsuchikawa, *J. Near Infrared Spec.* **2018**, 26, 53.
- [28] I. Bargigia, A. Nevin, A. Farina, A. Pifferi, C. D'Andrea, M. Karlsson, P. Lundin, G. Somesfalean, S. Svanberg, *J. Near Infrared Spec.* **2013**, 21, 259.
- [29] I. Arganda-Carreras, V. Kaynig, C. Rueden, K. W. Eliceiri, J. Schindelin, A. Cardona, H. Sebastian Seung, *Bioinformatics* **2017**, 33, 2424.
- [30] J. A. Stratton, L. J. Chu, *Phys. Rev.* **1939**, 56, 99.
- [31] P. Monk, *COMPEL-The International Journal for Computation and Mathematics in Electrical and Electronic Engineering*, **1995**.
- [32] J. P. Berenger, *J. Comput. Phys.*, James & James Science Publishers Ltd, **1995**, 14, 41.
- [33] A. Samanta, H. Chen, P. Samanta, S. Popov, I. Sychugov, L. A. Berglund, *ACS Appl. Mater. Interfaces* **2021**, 13, 3270.